

Propagation Model Based on Ray Tracing for the Design of Personal Communication Systems in Indoor Environments

Francisco Saez de Adana, Oscar Gutiérrez Blanco, Iván González Diego, Jesús Pérez Arriaga, and Manuel F. Cátedra

Abstract—In this paper, a ray-tracing technique to predict the propagation channel parameters in indoor scenarios is presented. It is a deterministic technique, fully three-dimensional, based on geometrical optics (GO) and the uniform theory of diffraction (UTD). A model of plane facets is used for the geometrical description of the environment. The ray tracing is accelerated considerably by using the Angular Z-Buffer algorithm. Some comparisons between predicted results and measurements are presented to validate the method.

I. INTRODUCTION

THE STUDY of the propagation in indoor environments has increased enormously in recent years, the main reason being the large amount of competition that exists in mobile communications at the moment. This makes it necessary to have a way to predict the propagation in indoor environments in order to carry out a prior analysis, which allows us to minimize the number of base stations required to give an efficient service, with the economical saving that it represents. Another factor that in the future will be of great interest in the designs is the limiting of the field level to a very restrictive low level in order to comply with public health regulations.

It is very important to study how the different elements that make up the buildings affect the propagation. The main problem that appears is the fast fading [1] caused by multipath propagation and the interference between the different paths. This makes it very difficult to obtain good predictions at the received power levels. However, due to its practical interest, in recent years, many researchers have developed different models with which to study indoor propagation.

Traditionally, statistical models have been used for this problem [2]–[4]. For instance, the empirical model that predicts the propagation path loss on the same floor or through different floors is shown in [2]. A more sophisticated method that considers the attenuation through individual walls and floors is presented in [3]. A nonlinear function of the number of penetrated floors is introduced in [4] to fit the measurements better than in previous models.

At the moment, deterministic models are becoming more popular [5]–[10]. For example, we can start by mentioning [5], where a computer tool to predict path loss inside buildings

based on geometrical optics is reported. In [6], Valenzuela estimates the local mean signal strength at a point as the sum of the reflected and transmitted rays that reach that point. In [7], results of hallway environments are shown using a method that takes into account the material properties of the elements of the building. Kajiwira shows the importance of polarization in indoor propagation in [8], demonstrating that a circular polarized wave can reduce the multipath fading. A theoretical model for the analysis of corridor environments is presented in [9]. A three-dimensional (3-D) propagation model, combined with a patched-wall model, to predict radio losses in a corridor environment is detailed in [10]. These models are based on the ray tracing, determining the channel parameters taking into account the rays that, following different paths, reach the receiver antenna. The main problem of ray tracing is the high amount of CPU-time required to analyze the large amount of rays that can reach a point after several reflections and transmissions.

In this work, a fully 3-D model based on geometrical optics (GO) and the uniform theory of diffraction (UTD) is presented. The geometrical representation of the elements in an indoor environment is based on plane facets. The influence of the electromagnetic properties of the material of each facet is included in the expressions of GO and UTD and the transmission through the walls is also included, as it has a very important effect on this application.

As mentioned earlier, the problem with these ray-tracing models is the high simulation time that they require. The reason is the large amount of intersection tests needed to find out if a ray hits a facet, as the number of facets used to represent a building can be very high. In this paper, we describe a very efficient ray-tracing technique for indoor environments, the Angular Z-Buffer (AZB), which allows a reduction in the time necessary to obtain the multipath propagation. The philosophy behind this method consists in reducing the number of rigorous tests that have to be made by reducing the number of facets that each ray has to treat.

A code called FASPRI has been created using this electromagnetic method combined with the AZB. The efficiency of the ray-tracing technique enables this code to be run on a PC. Some results obtained with this code compared with measurements are presented to show the accuracy of the method.

This paper is organized as follows. In Section II, the propagation model is presented. In Section III, the geometrical model used to represent the indoor environment is outlined. The AZB applied to this case is described in Section IV. The validation results compared with measurements are shown in Section V.

Manuscript received December 3, 1999; revised March 30, 2000. This work was supported in part by Telefonica Móviles, Spain.

The authors are with Grupo de Servicios, Universidad de Alcalá, Alcalá de Henares 28806 Spain (e-mail: felipe.catedra@alcala.es).

Publisher Item Identifier S 0018-9545(00)09179-9.

Finally, the conclusions of this work are presented at the end of this paper.

II. PROPAGATION MODEL

The propagation model is based on GO and the UTD [11], including the effects related to the transmission that is very important in these kinds of environments. These are asymptotic high-frequency theories, which obtain the total electric field at a point as the sum of the field associated with all the rays that reach this point. The following effects, which are considered enough to obtain good results in indoor propagation, are included in this model:

- 1) direct field;
- 2) single-reflected field;
- 3) single-diffracted field;
- 4) transmitted field up to four transmissions
- 5) double-reflected field;
- 6) single-reflected single-diffracted and single-diffracted single-reflected field;
- 7) single-reflected-transmitted and transmitted-single-reflected field, including up to three transmissions;
- 8) double-reflected-transmitted and transmitted-double-reflected field, including up to two transmissions.

In indoor environments, the elements of the geometry can be composed of different materials. In this part, the method for obtaining the field associated to each effect including the characteristics of the materials is presented.

A. Direct Field

The field contribution at the observation point (O) due to the direct ray is given by

$$\vec{E}(O) = \vec{E}_t(\theta, \phi) \frac{\exp(-jk_0 r)}{r} \quad (1)$$

where

$$\vec{E}_t(\theta, \phi) = \sqrt{\frac{\eta P_r G}{4\pi}} \vec{E}_o(\theta, \phi) \quad (2)$$

and

$k_0 = (2\pi)/\lambda$	free-space wavenumber with λ being the wavelength;
r	distance between the transmitter and the observation point;
η	free-space impedance;
P_r	power radiated by the transmitter;

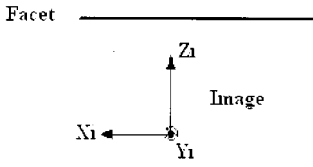
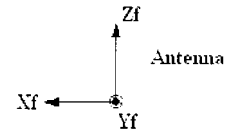


Fig. 1. Axis system to apply the image theory.

G	gain of the transmitter antenna;
$\vec{E}_o(\theta, \phi)$	normalized radiation pattern of the transmitter antenna;
θ and ϕ	spherical coordinates of the observation point referred to the coordinate system associated with the antenna.

B. Reflected Field

In this case, instead of the general expressions of GO, the image theory is applied [12]. This theory, usually presented for dipoles, can be generalized for other antennas defining an image axis system from the coordinate system of the antenna, as seen in Fig. 1. This system is defined by a translation of the facet-fixed axes, which are defined by making Z_f parallel to the normal vector of the facet, X_f parallel to one of the sides of the facet, and Y_f perpendicular to the other two axes [13].

Taking into account this new system and expressing the reflected field in its components parallel and perpendicular [11], the reflected field can be expressed as

$$\vec{E}_r(O) = \left\{ R_{||}(\theta_i) \vec{E}_{\theta f}(\pi - \theta_i, \phi_i) \hat{\theta}_i + R_{\perp}(\theta_i) \vec{E}_{\phi f}(\pi - \theta_i, \phi_i) \hat{\phi}_i \right\} \frac{\exp(-jk_0 r_i)}{r_i} \quad (3)$$

where

r_i	distance between the image and the observation point;
$\vec{E}_{\theta f}(\pi - \theta_i, \phi_i)$,	parallel and perpendicular components of the normalized radiation pattern of the transmitter antenna referred to the facet-fixed system;
$\vec{E}_{\phi f}(\pi - \theta_i, \phi_i)$	

$$R_{||} = \frac{(\varepsilon_r - \sin^2 \theta_i - \varepsilon_r^2 \cos^2 \theta_i) [\exp(2j dk_0 \sqrt{\varepsilon_r - \sin^2 \theta_i}) - 1]}{\exp(2j dk_0 \sqrt{\varepsilon_r - \sin^2 \theta_i}) (\sqrt{\varepsilon_r - \sin^2 \theta_i} + \varepsilon_r \cos \theta_i)^2 - (\sqrt{\varepsilon_r - \sin^2 \theta_i} - \varepsilon_r \cos \theta_i)^2} \quad (4)$$

$$R_{\perp} = \frac{(1 - \varepsilon_r) (\exp(2j dk_0 \sqrt{\varepsilon_r - \sin^2 \theta_i}) - 1)}{\exp(2j dk_0 \sqrt{\varepsilon_r - \sin^2 \theta_i}) (\cos \theta_i + \sqrt{\varepsilon_r - \sin^2 \theta_i})^2 - (\cos \theta_i - \sqrt{\varepsilon_r - \sin^2 \theta_i})^2} \quad (5)$$

θ_i and ϕ_i spherical coordinates of the observation point referred to the image coordinate system.

R_{\parallel} and R_{\perp} are the parallel and perpendicular reflection coefficients given in [14] and [15], as seen in (4) and (5) at the bottom of the page, where

- θ_i incident angle at the facet;
- d facet thickness;
- ϵ_r relative permittivity of the wall medium;
- k wave number of the wall medium

$$k = \frac{2\pi}{\lambda} \sqrt{\epsilon_r}. \quad (6)$$

C. Transmitted Field

The expression for the transmitted field is very similar to that used for the reflected field, but taking as its origin the transmitter antenna instead of the image and taking into account the transmission coefficients. The transmitted field is given by

$$\vec{E}_t(O) = \left\{ T_{\parallel}(\theta_i) E_{\theta}(\theta, \phi) \hat{\theta} + T_{\perp}(\theta_i) E_{\phi}(\theta, \phi) \hat{\phi} \right\} \frac{\exp(-jk_0 r)}{r} \quad (7)$$

where

- r distance between the transmitter antenna and the observation point;
- $\vec{E}_{\theta}(\theta, \phi), \vec{E}_{\phi}(\theta, \phi)$ parallel and perpendicular components of the normalized radiation pattern of the transmitter antenna;
- θ and ϕ spherical coordinates of the observation point referred to the coordinate system associated with the antenna.

T_{\parallel} and T_{\perp} are the parallel and perpendicular transmission coefficients given in [14] and [15], as seen in (8) and (9) at the bottom of the page.

D. Diffracted Field

To obtain the field diffracted by an edge, the general expressions of the UTD are used [11], but including the influence of the materials. Therefore, the diffraction coefficients [11] are as follows:

$$D_{\parallel, \perp} = D_1 + D_2 + R_{\parallel, \perp}(D_3 + D_4) \quad (10)$$

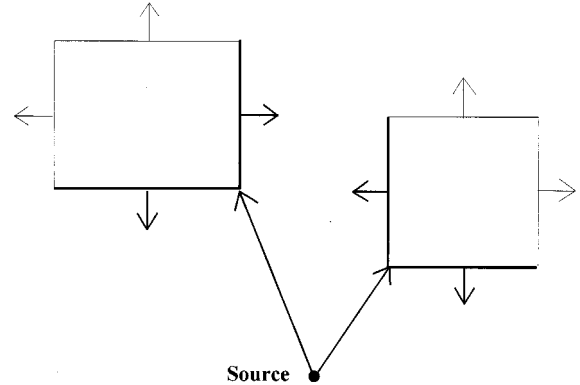


Fig. 2. Bold line: facets that satisfy the normal vector criterion.

where

- D_1, D_2, D_3 , and D_4 components of the diffraction coefficients given in [11];
- $R_{\parallel, \perp}$ reflection coefficients given by (4) and (5).

E. Multiple Effects

The second and higher order effects are computed as a combination of the previous effects [11].

III. GEOMETRICAL MODEL

A model of plane facets is used to describe the indoor geometries. All the elements of an indoor emplacement such as walls, columns, doors, etc., are represented by facets with three or four vertices. In this model, the electric permittivity (ϵ), the conductivity (σ), and the thickness of each facet are introduced as input data.

The number of facets necessary to model a complex environment with enough precision can be of several hundred facets. Therefore, the number of intersection tests required to find the ray paths can be very high, its computation taking a lot of CPU time. So, a geometrical preprocessing has been chosen to reduce this time. This process consists of computing the normal vectors to the facets in order to introduce a criterion, which allows a reduction of approximately 50% of the number of facets that have to be considered. This criterion only considers the facets facing from the source, which are those that satisfy the criterion

$$\hat{n} \cdot \vec{r} \leq 0 \quad (11)$$

where

- \hat{n} normal vector to the facet;

$$T_{\parallel} = \frac{4\epsilon_r \sqrt{\epsilon_r - \sin^2 \theta_i} \cos \theta_i \exp[jdk_0 (\sqrt{\epsilon_r - \sin^2 \theta_i} + \cos \theta_i)]}{\exp(2j dk_0 \sqrt{\epsilon_r - \sin^2 \theta_i}) (\epsilon_r \cos \theta_i + \sqrt{\epsilon_r - \sin^2 \theta_i})^2 - (\sqrt{\epsilon_r - \sin^2 \theta_i} - \epsilon_r \cos \theta_i)^2} \quad (8)$$

$$T_{\perp} = \frac{4\sqrt{\epsilon_r - \sin^2 \theta_i} \cos \theta_i \exp[jdk_0 (\sqrt{\epsilon_r - \sin^2 \theta_i} + \cos \theta_i)]}{\exp(2j dk_0 \sqrt{\epsilon_r - \sin^2 \theta_i}) (\sqrt{\epsilon_r - \sin^2 \theta_i} + \cos \theta_i)^2 - (\cos \theta_i - \sqrt{\epsilon_r - \sin^2 \theta_i})^2} \quad (9)$$

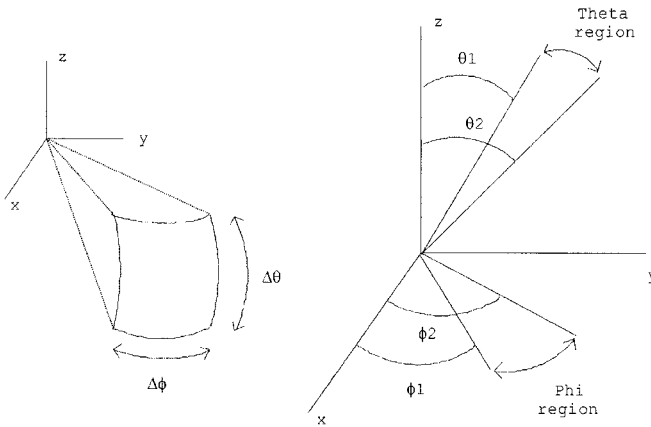


Fig. 3. Regions of theta and phi that form a Z-buffer anxel.

\vec{r} vector that joins the source to one of the vertices of the facet.

An example is depicted in Fig. 2. The facets that satisfy the criterion are represented with a bold line.

But for a complicated model, this criterion is not enough for an efficient analysis, other techniques to optimize the ray tracing should be introduced.

IV. THE ANGULAR Z-BUFFER

In this method, the AZB algorithm [16] is used to speed up the ray tracing. This algorithm is based on the light buffer technique [17] used in computer-aided graphic design. The AZB consists in dividing the space seen from the source in angular regions and storing the facets of the model in the regions where they belong. In this way, for each ray, only the facets stored in its region need be analyzed. Another important trick to reduce the computation time is to order the facets in each region according to their distances from the source, since the closer facets have more possibility of hiding rays.

A. Application to Direct Ray

For the direct ray, the source will be the transmitter antenna. In this case, the space regions are spherical sectors, which we call anxels, defined by their spherical coordinates θ and ϕ , as illustrated in Fig. 3.

Each region is obtained by dividing the 2π radians of ϕ and the π radians of θ in equal parts. Therefore, the width of the anxels will be

$$\Delta\theta = \frac{\pi}{nr_\theta}; \quad \Delta\phi = \frac{2\pi}{nr_\phi} \quad (12)$$

where

nr_θ number of regions in theta;

nr_ϕ number of regions in phi.

For all vertices of all the facets of the model, the maximum and minimum values of the coordinates θ and ϕ are computed. It is assumed that each facet belongs to all the anxels between these minimum and maximum values.

This information is very efficient to compute the hiding of a direct ray. The first step is to determine the anxel of the ray

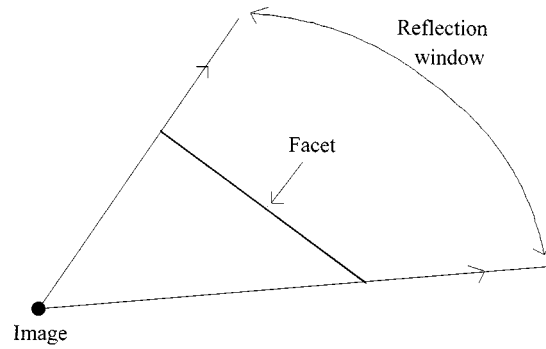


Fig. 4. Two-dimensional view of the angular window where the reflection can be produced.

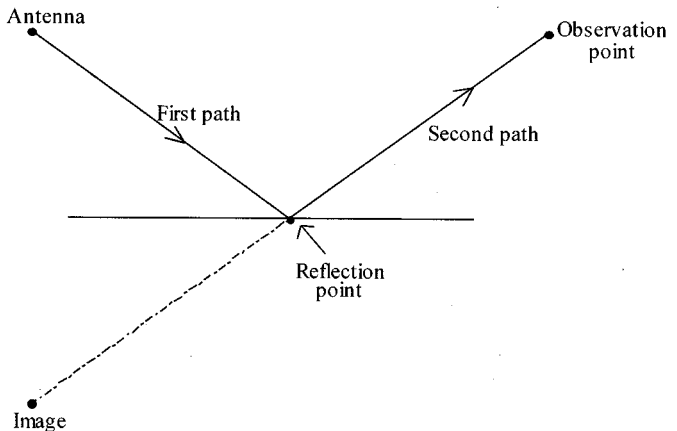


Fig. 5. Two paths of a reflected ray.

using its spherical coordinates. Then the facets loaded in this region are tested in the order in which they are stored (according to the distance from the source). If one facet intersects the ray, the algorithm is stopped and the ray contribution is not taken into consideration. If no facet hides the ray, the electric field is computed at the observation point.

B. Application to Reflected Ray

The algorithm for this case is applied in the same way but taking as its source the image of each facet. The anxels are also spherical sectors, but now are limited to lie in the angular window region where the reflection can be produced. This window is defined in Fig. 4.

In this case, to check the obstruction of the rays, two paths must be considered: one from the transmitter antenna to the reflection point and the other, from this, to the receiver or observation point, as shown in Fig. 5.

So the intersection test must be done for both paths. For the first one, the AZB of the direct ray is used, and for the second one, the AZB of the reflected ray is used.

C. Application to Transmitted Ray

In this case, there are two paths, as in the reflection case: one from the source to the transmission point in the facet and the other from this to the observer. For the second path, the AZB is created in the same way as in the direct case but taking as its source the transmission point.

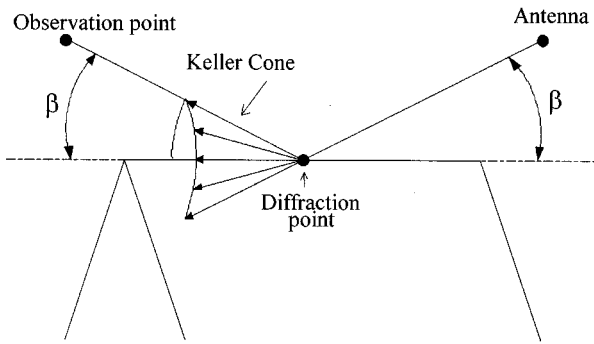


Fig. 6. Keller's cone, which defines the β coordinate for the Z-buffer for diffraction.

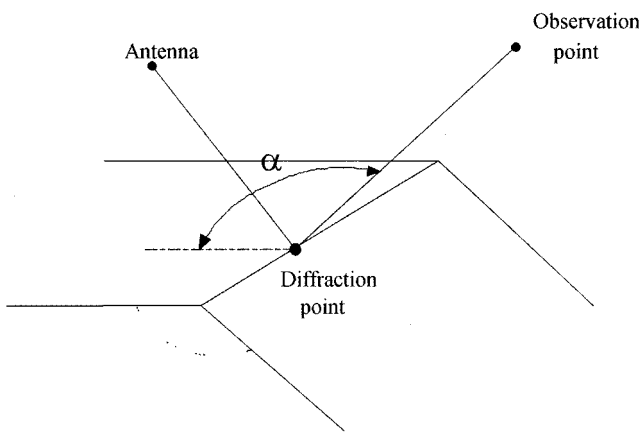


Fig. 7. Angle α used to define the other coordinate in the Z-buffer for diffraction.

D. Application to Diffracted Ray

For the diffracted ray case, instead of working with spherical coordinates θ and ϕ , it is easier to work with coordinates β and α . The reason is that when a ray reaches a wedge forming an angle β with its edge, the diffracted rays are contained in a cone (Keller's cone [18]) with its axis on the edge, the vertex of which is the diffraction point and has an aperture angle equal to β (see Fig. 6). The other coordinate is given by the angle α , which is the angle between the diffracted ray and the first facet of the edge (see Fig. 7).

In this case, as in the reflection, a diffraction window is created by each edge. This window is defined between the angles β_{\min} , β_{\max} and α_{\min} , α_{\max} , where the edge can produce diffraction. The facets are stored in the corresponding anxels, taking the angles β and α of their vertices in a similar way as for the direct or reflected rays but now considering the coordinate system defined by α and β .

As in the previous effects, the intersection test is performed for two paths (Tx: diffraction point and Rx: diffraction point), the first one using the AZB of the direct case and the second one using the AZB created for the corresponding edge.

E. Application to Multiple Effects

For the multiple effects, the AZB is applied as a combination of the previous cases. For instance, for reflection-diffraction, the intersection test must be done for three paths. From the trans-

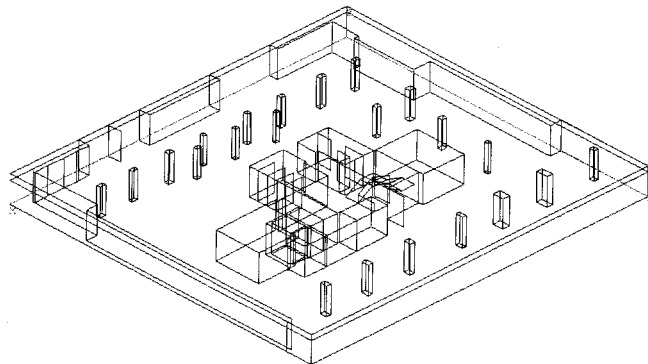


Fig. 8. 3-D view of the third floor of the Sota building.

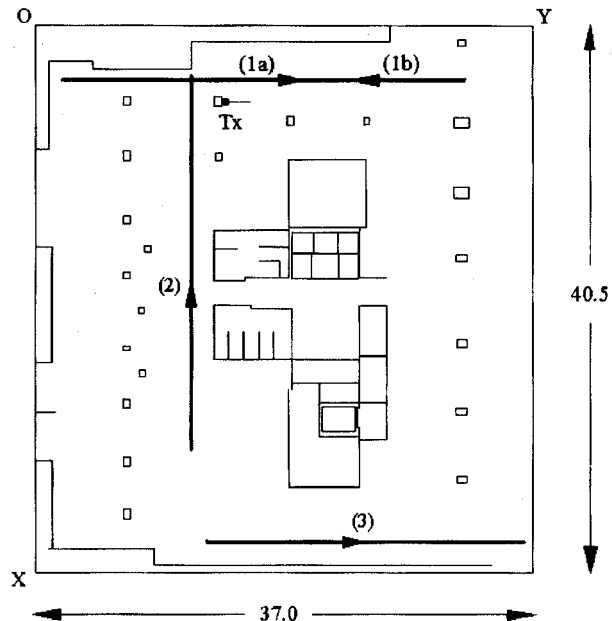


Fig. 9. Top view of the third floor of the Sota building. The bold lines indicate the paths considered for the analysis when the transmitter (Tx) is in the position shown (taken from [19]).

mitter antenna to the reflection point, the AZB created for the direct ray is used. From the reflection point to the diffraction point, the AZB created for the image is checked. Finally, from the diffraction point to the receiver, the AZB created by the edge is considered.

Although multiple diffraction has not been considered in this description, the algorithm can be also apply to these effects. For example, for a double diffraction, the AZB would be created for the second edge as in a simple diffraction, but in this case the source is not a point but a line that corresponds with the first edge where the diffraction is produced. Following the same procedure, it could be applied for multiple diffraction.

V. VALIDATION

To validate the method, a set of measurements was made on the third floor of the Sota building in Bilbao, Spain. They were compared with code FASPRI based on the approach presented in this paper. The geometrical model of this floor is shown in Fig. 8. It is modeled by 175 facets, which include the floor and ceiling, in order to consider the reflections produced in both. All

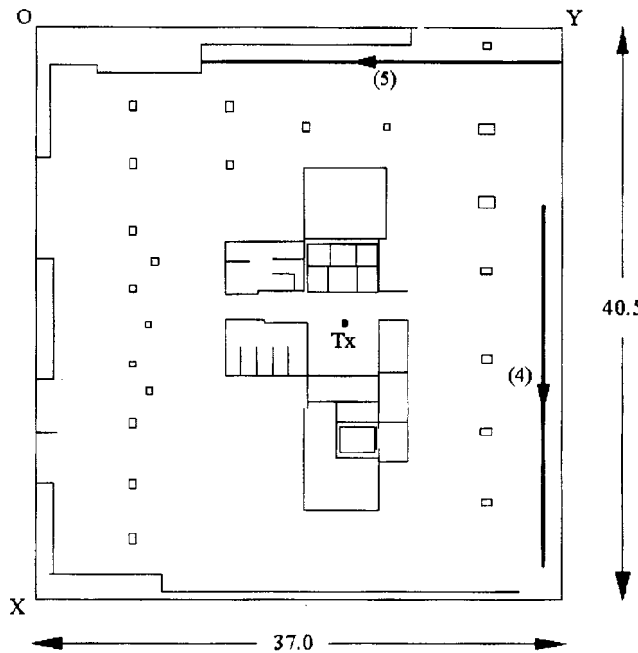


Fig. 10. Plan view of the third floor of the Sota building. The bold lines indicate the paths considered for the analysis when the transmitter (Tx) is in the position shown (taken from [19]).

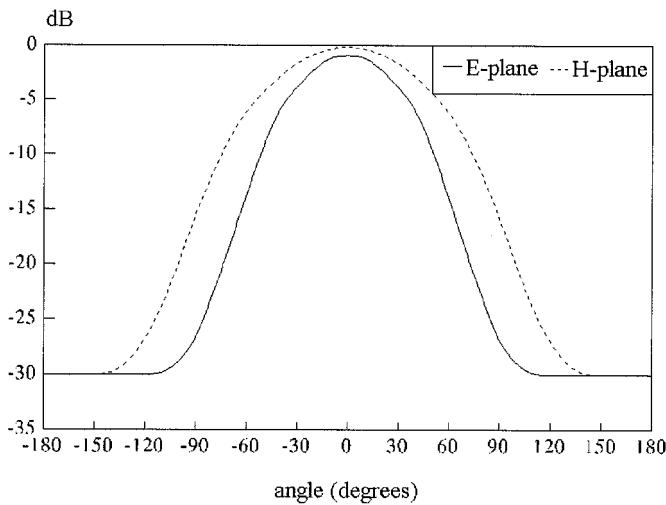


Fig. 11. *E*-plane and *H*-plane of the transmitter antenna used in the validation cases (taken from [19]).

the facets were assumed to be made of brick ($\epsilon_r = 4.44$, $\sigma = 0.08$ S/m, $\mu_r = 1.0$) with a thickness of 0.1 m. The frequency considered was 950 MHz.

The receiver power measurements were made along several straight paths for two different locations of the transmitter antenna. These measurements (and, therefore, the FASPRI results) were not averaged. Reflections on floor and ceiling were considered. The paths for the first antenna position are depicted in Fig. 9 and for the second one in Fig. 10. The dimensions of the scene are given in meters. The second path (line 2 in Fig. 9) is 28.3 m. The results obtained for this path are shown in Fig. 14.

The transmitter antenna is vertically polarized, and its radiation pattern can be seen in Fig. 11. The transmitter power is 23 dBm, and the antenna gain is 7 dBi.

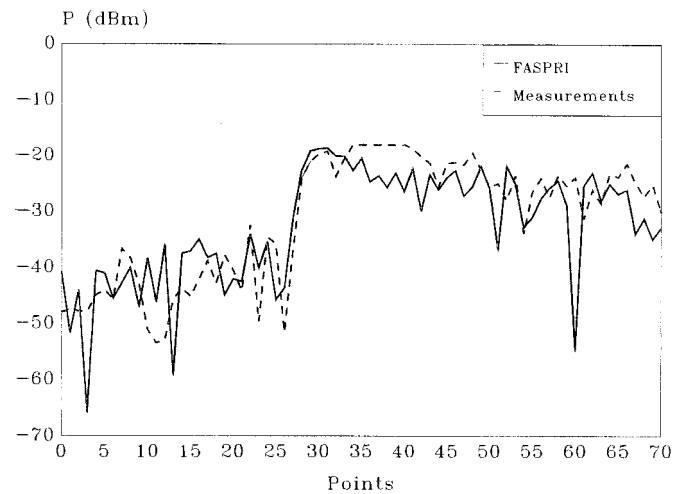


Fig. 12. Comparison between measurements and simulation for path 1 of Fig. 9. The first point corresponds to the left side of the path (taken from [19]).

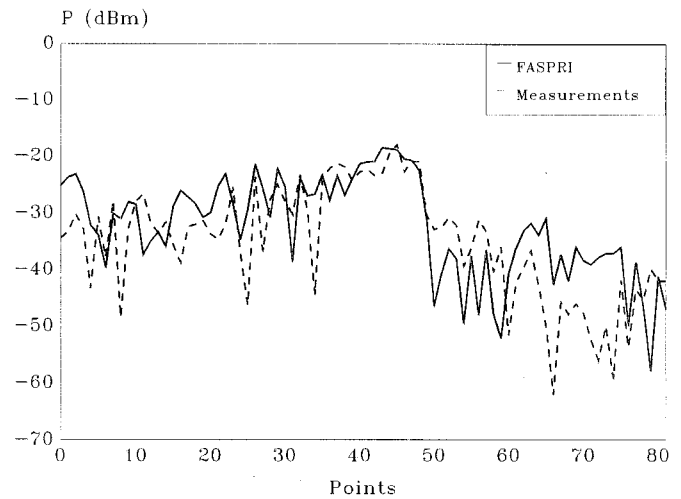


Fig. 13. Comparison between measurements and simulation for path 1 of Fig. 9. The first point corresponds to the right side of the path (taken from [19]).

In the first three cases, the transmitter antenna is placed on a column at (5.67, 13.85, 1.7), and its direction of maximum radiation is along the *Y* axis. The first path (line 1 in Fig. 9) is a line-of-sight (LOS) path with a length of 30 m. The measurements were made in both directions: right to left and left to right. The results of both are shown in Figs. 12 and 13.

The third path (line 3 in Fig. 9) is a no-LOS (NLOS) path with a length of 23 m. Fig. 15 presents the results obtained compared with measurements.

Two more measurements were made with the same antenna placed on the ceiling (21.0, 21.0, 2.85), as shown in Fig. 10. The maximum radiation of the antenna is, in this case, along the $-Z$ axis. The simulation results compared with the measurements for the fourth path (line 4 in Fig. 10) can be seen in Fig. 16. This path is 25.7 m long.

The fifth path (line 5 in Fig. 10) is again an NLOS situation. Its length is 25.3 m. The results are depicted in Fig. 17.

All the cases seen previously were run on a Pentium 333 MHz with 128 MB of RAM. The CPU time required for each one is shown in Table I. This time is compared with that obtained

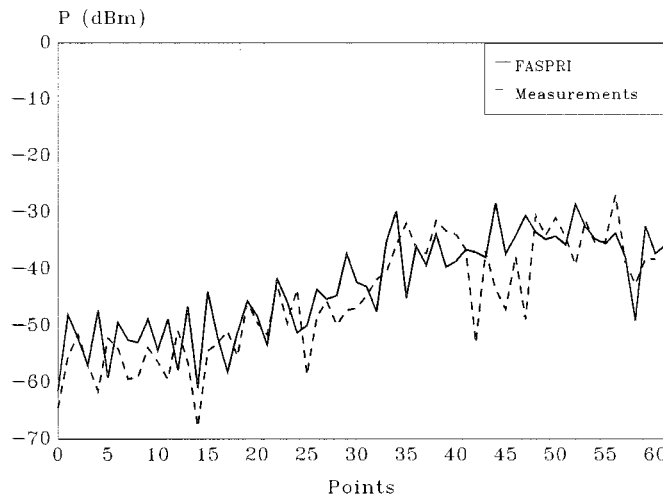


Fig. 14. Comparison between measurements and simulation for path 2 of Fig. 9 (taken from [19]).

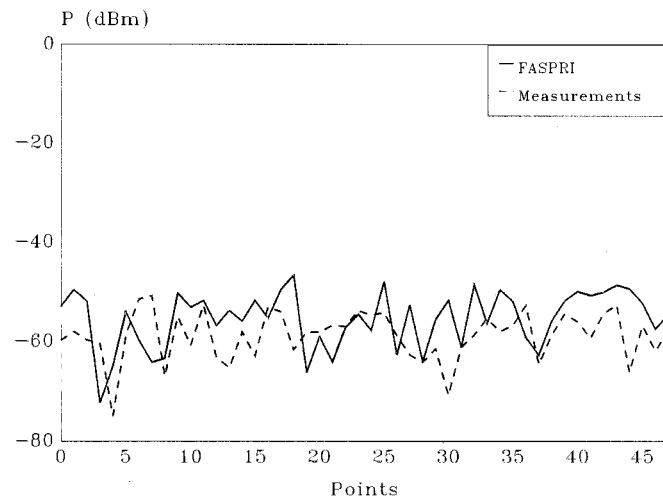


Fig. 15. Comparison between measurements and simulation for path 3 of Fig. 9 (taken from [19]).

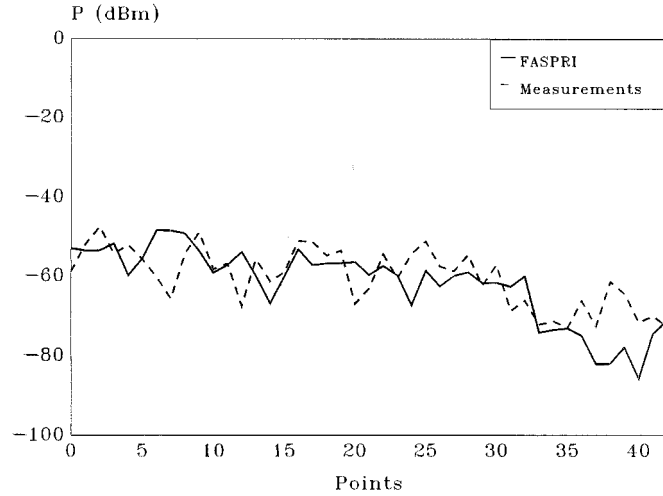


Fig. 16. Comparison between measurements and simulation for path 4 of Fig. 10 (taken from [19]).

using “brute force” for the ray tracing, that is to say, asking all the facets of the model about a possible hiding.

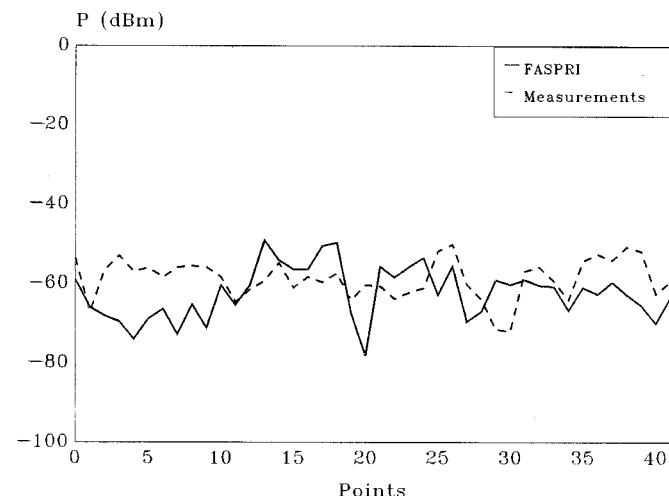


Fig. 17. Comparison between measurements and simulation for path 5 of Fig. 10 (taken from [19]).

TABLE I
COMPUTATION TIME REQUIRED FOR EACH PATH WITH AND WITHOUT AZB

Caption Path	Number of Points	Time using AZB	Time without AZB	Reduction
1 (right to left)	72	9min 21sec	2h 8min 5sec	92.7%
1 (left to right)	82	10min 33sec	3h 1min 54sec	94.2%
2	63	8min 19sec	1h 39min	91.6%
3	49	5min 56sec	1h 32min 42 sec	93.6%
4	42	5min 31sec	1h 8min 57sec	92%
5	42	5min 40sec	1h 22min 7 sec	93.1%

TABLE II
MEAN ERROR PREDICTIONS AND STANDARD DEVIATIONS FOR THE SIX PATHS ANALYZED

Caption Path	Mean error	Standard deviation
1 (right to left)	-1.37	7.04
1 (left to right)	2.57	8.32
2	1.65	7.96
3	3.38	6.79
4	-1.66	7.29
5	-3.55	8.33

Therefore, on average, this method consumes 8 min of CPU time for each point analyzed, reducing by more than 90% the time required doing the same analysis using the traditional GO/UTD.

Table II shows the mean error and standard deviation of the computed values regarding measurements. Predicted values appear to be reliable for engineering purposes in all the cases considered.

VI. CONCLUSIONS

A deterministic method for the analysis of indoor propagation has been presented. This method is based on GO/UTD. The main advantage of the method is the low simulation time that it requires by using the angular Z-buffer technique to speed up the

ray tracing, comparing the computation time with that necessary for the same analysis without AZB. The accuracy of the method has been tested obtaining some computed results in a real environment and comparing them with measurements. These tests have been done in LOS and NLOS situations.

REFERENCES

- [1] H. Hashemi, "The indoor radio propagation channel," *Proc. IEEE*, vol. 81, pp. 943–968, July 1993.
- [2] S. Y. Seidel and T. S. Rappaport, "914 MHz path loss prediction models for indoor wireless communications in multifloored buildings," *IEEE Trans. Antennas Propagat.*, vol. 40, pp. 207–217, Feb. 1992.
- [3] A. J. Motley and J. M. P. Keenan, "Radio coverage in buildings," *Br. Telecom Technological J. (Special Issue Mobile Communications)*, vol. 8, pp. 19–24, 1990.
- [4] C. Tornevik, J. E. Berg, and F. Lotse, "900 MHz propagation measurements and path loss models for different indoor environments," in *Proc. IEEE VTC'93*, 1993.
- [5] S. Y. Seidel and T. S. Rappaport, "A ray tracing technique to predict path loss and delay spread inside buildings," in *Proc. IEEE GLOBECOM'92 Conf.*, Orlando, FL, Dec. 1992, pp. 649–653.
- [6] R. A. Valenzuela, "A ray tracing approach to predicting indoor wireless transmission," in *Proc. IEEE Vehicular Technology Conf.*, 1993, pp. 214–218.
- [7] S. Y. Seidel and T. S. Rappaport, "Site-specific propagation prediction for wireless in-building personal communication system design," *IEEE Trans. Veh. Technol.*, vol. 43, no. 4, pp. 879–892, 1994.
- [8] A. Kajiwara, "Line-of-sight indoor radio communication using circular polarized waves," *IEEE Trans. Veh. Technol.*, vol. 44, no. 3, pp. 487–493, 1995.
- [9] G. M. Whitman, K. S. Kim, and E. Niver, "A theoretical model for radio signal attenuation inside buildings," *IEEE Trans. Veh. Technol.*, vol. 44, no. 3, pp. 621–629, 1995.
- [10] J. H. Tarn, W. R. Chang, and B. J. Hsu, "Three-dimensional modeling of 900 MHz and 2.44 GHz radio propagation in corridors," *IEEE Trans. Veh. Technol.*, vol. 46, pp. 519–526, May 1997.
- [11] D. A. McNamara, C. W. I. Pistorius, and J. A. G. Malherbe, *Introduction to the Uniform Geometrical Theory of Diffraction*. Reading, MA: Artech House Microwave, 1989.
- [12] C. A. Balanis, *Advanced Engineering Electromagnetics*. New York: Wiley, 1989.
- [13] J. Pérez and M. F. Cátedra, *Cell-Planing for Personal Communications*. Reading, MA: Artech House, 1999.
- [14] J. A. Stratton, *Electromagnetic Theory*. New York: McGraw-Hill, 1941.
- [15] W. C. Chew, *Waves and Fields in Inhomogeneous Media*. New York: IEEE Press, 1995.
- [16] M. F. Cátedra, J. Pérez, F. Saez de Adana, and O. Gutiérrez, "Efficient ray-tracing technique for three-dimensional analyzes of propagation in mobile communications: Application to picocell and microcell scenarios," *IEEE Antennas Propagat. Mag.*, vol. 40, pp. 15–28, Apr. 1998.
- [17] E. A. Hines and D. P. Greenberg, "The light buffer: A shadow testing accelerator," *IEEE Comput. Graph. Animat.*, pp. 6–16, Sept. 1986.
- [18] J. B. Keller, "Geometrical theory of diffraction," *J. Opt. Soc. Amer.*, vol. 52, no. 2, pp. 116–130, Feb. 1962.
- [19] M. F. Cátedra and J. Pérez, *Cell Planning for Wireless Communications*. Reading, MA: Artech House, 1999.

Francisco Saez de Adana was born in Santander, Spain, in 1972. He received the B.S. and M.S. degrees in telecommunications engineering from the University of Cantabria, Spain, in 1994 and 1996, respectively, where he is pursuing the Ph.D. degree in the Communications Engineering Department.

He has been an Assistant Professor in the Signal Theory and Communications Department of the University of Alcalá since 1998. He has participated in several research projects with Spanish and European companies, related to analysis of onboard antennas, radio propagation in mobile communication, and RCS computation. He has published two papers and more than ten conference contributions at international symposia. His research interests are in areas of high-frequency methods in electromagnetic radiation and scattering, on-board antennas analysis, radio propagation on mobile communications, and ray-tracing acceleration techniques.

Oscar Gutiérrez Blanco was born in Torrelavega, Spain, in 1970. He received the B.S. and M.S. degrees in telecommunications engineering from the University of Cantabria, Spain, in 1993 and 1996, respectively. He currently is pursuing the Ph.D. degree at the Signal Theory and Communications Department, University of Alcalá, Spain.

From 1995 to 1998, he was with the Communications Engineering Department of the University of Cantabria. He has participated in several research projects with Spanish and European companies related to analysis of on-board antennas, radio propagation in mobile communication, and RCS computation. His research interests are in high-frequency methods in electromagnetic radiation and scattering and ray-tracing acceleration techniques.

Iván González Diego was born in Torrelavega, Spain, in 1971. He received the B.S. and M.S. degrees in telecommunications engineering from the University of Cantabria, Spain, in 1994 and 1997, respectively. He currently is pursuing the Ph.D. degree at the Signal Theory and Communications Department, University of Alcalá, Spain.

From 1996 to 1998, he was with the Communications Engineering Department, University of Cantabria. He is an Assistant Professor with Alfonso X El Sabio University, Madrid, Spain. He has participated in several research projects with Spanish and European companies related to analysis of on-board antennas, radio propagation in mobile communication, and RCS computation. His research interests are in numerical methods applied to the electromagnetic problems, such as genetic algorithms and numerical methods to represent complex bodies for the electromagnetic techniques.

Jesús Pérez Arriaga received the M.S. and Ph.D. degrees in applied physics from the University of Cantabria, Spain.

In 1989, he was with the Radiocommunication and Signal Processing Department, Polytechnic University of Madrid, as a Research Assistant. From 1990 to 1992, he was with the Electronics Department, University of Cantabria, as a Research Assistant. In 1993, he became an Assistant Professor in the Electronic Department, University of Cantabria. Since October 1998, he has been an Assistant Professor at the University of Alcalá, Madrid, Spain. He has participated in more than 20 research projects related to RCS computation and performed analysis of on-board antennas and radio propagation in mobile communications. He is the author of one book, ten papers, and more than 25 conference contributions at international symposia. His research interests include high-frequency methods in electromagnetic radiation and scattering and mobile communications.



Manuel F. Cátedra received the M.S. and Ph.D. degrees in telecommunications engineering from the Polytechnic University of Madrid (UPM), Spain, in 1977 and 1982, respectively.

From 1976 to 1989, he was with the Radiocommunication and Signal Processing Department, UPM, teaching and doing research. He was a Professor at the University of Cantabria from 1989 to 1998. He is currently a Professor at the University of Alcalá, Madrid. He has worked on about 25 research projects solving problems of electromagnetic compatibility in radio and telecommunication equipment, antennas, microwave components, and radar cross section and mobile communications. He has developed and applied CAD tools for radio-equipment systems such as navy ships, aircraft, helicopters, and satellites, the main contractors being Spanish or European Institutions such as CASA, ALCATEL, DASA, SAAB, INTA, BAZAN, the Spanish Defense Department, and the French company MATRA. He is working now on projects for Telefonica (the largest Spanish telecommunication company) to develop computer tools for propagation analyses in microcells and indoor cells. He has directed about a dozen Ph.D. dissertations; has published about 35 papers, two books, and about ten book chapters; has given short courses; and has given around 100 presentations in international symposia.